Materials & Design 208 (2021) 109915

Contents lists available at ScienceDirect

Materials & Design

journal homepage: www.elsevier.com/locate/matdes

Mechanical, magnetic and magnetostrictive properties of porous Fe-Ga films prepared by electrodeposition

Aliona Nicolenco [a,b], Yu Chen [a], Natalia Tsyntsaru [b,c], Henrikas Cesiulis [c,d], Eva Pellicer [a,*], Jordi Sort [a,e,*]

[a] Departament de Física, Universitat Autònoma de Barcelona, Bellaterra, Spain
[b] Institute of Applied Physics, Chisinau, Republic of Moldova
[c] Vilnius University, Physics Department, Vilnius, Lithuania
[d] JSC Elektronikos perdirbimo technologijos, Vilnius, Lithuania
[e] Institució Catalana de Recerca i Estudis Avançats, Pg. Lluís Companys 23, 08010 Barcelona, Spain

HIGHLIGHTS

- Fe-Ga films with variable composition and porosity levels are electro deposited.
- Both hardness and Young's modulus decrease as the porosity degree increases.
- Highly tunable magnetic properties are achieved by adjusting the microstructure.
- Macroporous films show larger magnetic-field-induced crystal lattice deformation.

GRAPHICAL ABSTRACT

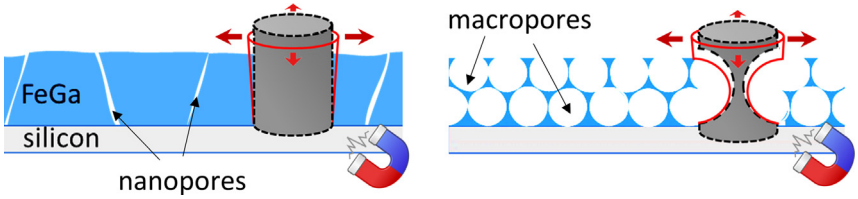

ARTICLE INFO

Article history:
Received 31 March 2021
Revised 24 May 2021
Accepted 16 June 2021
Available online 18 June 2021

Keywords:
Electrodeposition
Fe-Ga alloy
Porous films
Nanoindentation
Magnetostriction

ABSTRACT

Magnetostriction, known as the ability of magnetic materials to expand or contract in response to magnetic field, is a key property of Fe-Ga alloys exploited in various types of transducers. Usually, thin films of Fe-Ga deposited on rigid substrates suffer from a clamping effect that hinders the propagation of strain. Herein, Fe-Ga films with macroporous, not fully constrained, geometry are prepared by electrodeposition on metallized silicon substrates templated with sub-micrometer-sized polystyrene spheres. For comparison, fully-dense and inherently nanoporous films are prepared by sputtering and electrodeposition, respectively. The electrodeposition mechanism is discussed in terms of electrochemically active species distribution and partial current densities. The composition of the Fe-Ga films has been tuned (2–40 at.% Ga) by varying the electrodeposition parameters. A complete assessment of the nanomechanical and magnetic properties of the films with variable composition and porosity has been performed for an optimized performance. The magnetostriction has been studied by X-ray diffraction applying an in-situ magnetic field. The results demonstrate a larger magnetic-field-induced crystal deformation in templated (macroporous) films compared to the non-templated and fully-dense counterparts. The observed effects in porous Fe-Ga films are very appealing for the design of various strain-engineered nanomaterials, e.g., energy transducers or magnetoelectric composites.

© 2021 The Author(s). Published by Elsevier Ltd. This is an open access article under the CC BY-NC-ND license (http://creativecommons.org/licenses/by-nc-nd/4.0/).

1. Introduction

Magnetostriction is a property of ferro- and ferrimagnets that allows these materials to expand or contract in response to a magnetic field due to the reorientation of magnetic domains. Essen-

* Corresponding authors at: Departament de Física, Universitat Autònoma de Barcelona, Bellaterra, Spain (J. Sort).
E-mail addresses: Eva.Pellicer@uab.cat (E. Pellicer), Jordi.Sort@uab.cat (J. Sort).

https://doi.org/10.1016/j.matdes.2021.109915
0264-1275/© 2021 The Author(s). Published by Elsevier Ltd.
This is an open access article under the CC BY-NC-ND license (http://creativecommons.org/licenses/by-nc-nd/4.0/).

tially, these materials can convert the electromagnetic energy into vibrations or mechanical energy (and vice versa), an effect that can be exploited in sensors and actuators. The ability to induce strain (λ) in the material by using an external magnetic field is widely utilized in magnetoelectric (ME) composites to modulate the electric polarization of the adjacent ferroelectric phase (direct magnetoelectric effect). Recently, this technology has been applied for remote, non-invasive, electric stimulation of living cells (without implanted electrodes) [1], targeted drug delivery [2], energy harvesting systems [3] and water remediation [4], among others. The most magnetostrictive material known so far is Terfenol-D, an alloy of terbium, dysprosium, and iron. However, Terfenol-D is brittle and, generally, bulky in size. Having no rare-earth elements in the composition and enhanced mechanical properties compared to brittle Terfenol-D is highly desirable. In this sense, Fe-Ga is one of the most suitable alternative magnetostrictive materials for current micro-/nanofabrication technologies [5]. Moreover, Fe-Ga is biocompatible, which makes it suitable for biomedical applications [6,7].

Traditionally, magnetostrictive thin films suffer from a clamping effect when grown onto rigid substrates. This significantly hinders effective magnetic-field induced strain generation and transfer (in the case of ME composites) [8]. Therefore, the ability to design magnetostrictive thin film-based architectures at the micro-/nanoscales (e.g., high aspect ratio patterned structures where the interface contact area with the substrate is minimized) has become extremely valuable. Nonetheless, while the existence of homogeneous strains under the action of magnetic field in thin magnetostrictive films grown onto rigid substrates is a priori not expected (due to the clamping), a recent study from our group demonstrated the occurrence of strain-gradients (instead of homogeneous strains) in μm-thick Fe-Ga films prepared by electrodeposition onto metalized silicon [9]. The observed effect originated from the residual nanoporosity in between the columnar Fe-Ga grains that allowed each grain to exhibit a lateral compression, progressively larger with the increase in distance from the substrate, where the grains are physically clamped.

In spite of their potential interest, porous magnetostrictive materials have not been systematically studied yet, although the investigation of such materials is interesting for several reasons: (i) the magnetostriction of porous films deposited on rigid supports can be enhanced due to the absence of lateral constraints, ultimately leading to strain gradients instead of homogeneous strains, which might be interesting for, e.g., generation of flexoelectric or flexomagnetic effects [10,11]; (ii) porosity may offer several advantages when it comes to mechanical properties of the films, e.g., increase of the plasticity index, making the material eventually suitable for damping applications [12], or reduction of the Young's modulus, which is highly desirable in biomaterials targeted for orthopedic applications [13]; (iii) porous magnetostrictive matrices can accommodate guest materials inside their voids, e.g., ferroelectric oxides or polymers, thus producing large surface area ME composites [14] (this, so far, has been achieved mainly by loading nanoparticles into 3D porous matrices [15,16]), or exchange-coupled systems (e.g., spring magnets) [17].

Thin films of Fe-Ga can be deposited either by physical (e.g., sputtering) or, more rarely, electrochemical methods i.e., by electrodeposition from aqueous (citrate, gluconate, acetate, phosphate, etc.) or ionic liquid electrolytes [5,18–21]. Interestingly, compared to physical deposition methods, electrodeposition offers several significant advantages such as scalability and low cost (particularly when aqueous electrolytes, e.g., based on citrates, are used). Furthermore, electrodeposition is one of the most suitable methods for the fabrication of porous micro-/nanostructures [22–24]. Alloys with variable composition, crystallographic structure, and thickness (nm–μm) can be obtained by varying the electrodeposition parameters in a relatively easy manner at ambient temperature and pressure. Typically, electrodeposited Fe-Ga has a polycrystalline structure with a magnetostrictive coefficient up to 150 ppm depending on the composition, i.e., two maxima in magnetostriction are usually observed at around 20 at.% of Ga (also known as "galfenol") and at 30 at.% [5,25]. Magnetostriction can be higher in (100)-single crystal Fe-Ga ($3/2\lambda_{100} \approx 400$ ppm) [26], but polycrystalline alloys exhibit some superior mechanical properties (like higher resilience to yielding). It is worth mentioning that although the magnetostrictive properties of electrodeposited Fe-Ga alloys have been studied to some extent [18–20], investigation on the mechanism of Fe and Ga co-deposition that allows for stringent control over material's design remains rather elusive.

In this study, we propose an original way to maximize the functionality of Fe-Ga films grown onto rigid substrates while circumventing the problem of substrate clamping: to combine electrodeposition with colloidal lithography to purposely introduce different porosity levels in the films during their growth. The interrelationships between microstructure, porosity and composition in the obtained alloys have been established and correlated with the resulting mechanical, magnetic and magnetostrictive properties. The obtained results can lead to new strain-engineered nanomaterials concepts, with potential applications in diverse fields such as magnetoelectric materials for data storage, energy conversion or biomedicine.

2. Experimental

Fe-Ga films were electrodeposited from an electrolytic bath with the following composition: 0.015 M $FeSO_4$, 0.038 M $Ga_2(SO_4)_3$, 0.5 M Na_2SO_4 and 0.065 M $C_6H_8O_7$ (citric acid). The pH of the bath was varied between 3 and 5, by adding NaOH to the solution. Electrodeposition was performed in a standard single compartment double jacketed cell connected to a Metrohm/Eco Chemie Autolab PGSTAT302N potentiostat/galvanostat. Silicon substrates with an e-beam evaporated 10 nm Ti adhesion layer and a 90 nm Au seed layer (highly textured along (111) direction) were used as a working electrode. A double junction Ag/AgCl reference electrode (Metrohm AG) was used with 3 M KCl inner solution and 1 M Na_2SO_4 outer solution. A platinized titanium mesh served as a counter electrode. Prior to use, the substrates were cleaned in acetone, ethanol and Milli-Q water. To prepare the templated (macroporous) films, amidine functionalized polystyrene (PS) spheres of 400 nm in diameter (purchased from Thermo Fisher) were electrophoretically deposited on the substrate in a custom-made 2-electrode cell [23]. A constant potential of −30 V was applied for 2 min to allow for multilayer assembly of the spheres. Following the electrophoretic deposition, the samples were promptly placed on a hot plate and heated at 50 °C for 15 min to evaporate the solvent and stabilize the assembled sphere layers. Electrodeposition of Fe-Ga films was performed potentiostatically in the range from −1.20 to −1.35 V (vs. Ag/AgCl) for 15 min, at 25 °C. Mild stirring conditions were applied to enhance the mass transport of species from the bulk electrolyte towards the electrode surface. In the case of macroporous films, after Fe-Ga electrodeposition, PS spheres were removed by immersing the samples in tetrahydrofuran for 1 h followed by a final rinsing in acetone, ethanol, and Milli-Q water. Schematic drawings of the synthetic routes used to produce templated and non-templated Fe-Ga films are shown in Fig. 1. Continuous, fully dense, Fe-Ga films with 20 at.% Ga were also prepared by sputtering and used as control samples whenever needed. For this, an individual $Fe_{80}Ga_{20}$ (at.%) target was evaporated using a 150 W DC gun for 25 min.

The distribution of metal species in the electrolyte as a function of pH was calculated by solving an equation set, which included

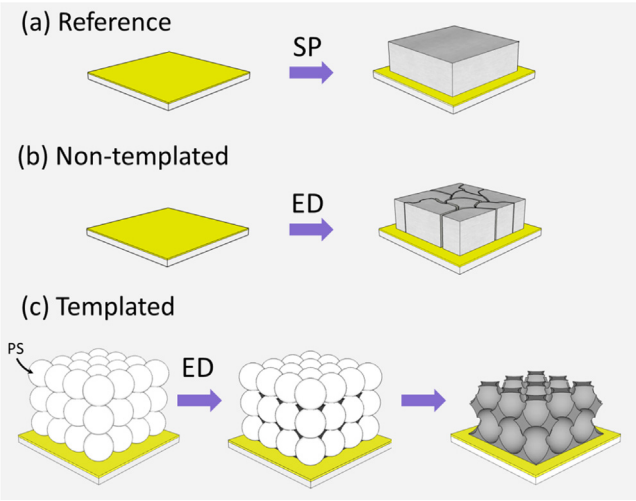

Fig. 1. Schematic illustration of the synthetic routes used to produce the Fe-Ga films: (a) sputter deposition, (b) potentiostatic electrodeposition onto a rigid substrate, and (c) two-step process involving electrodeposition through colloidal template followed by the template removal. "SP" – sputtering, "ED" – electrodeposition, "PS" – polystyrene spheres.

the following relations and quantities: (i) the equilibrium constants for all compounds added to or formed in solution, using values listed in **Table S1**; (ii) the mass balance equations for all forms in the equilibrium mixture (Eq. (1)), and (iii) the charge balance equation, where "Cat" and "An" denote cation and anion, respectively (Eq. (2)).

$$[J]_{tot} = \sum [J_i^{n+/-}] \quad (1)$$

$$\sum n_i [Cat_i^{n+}] = \sum n_i [An_i^{n-}] \quad (2)$$

where J is the species and n is the charge. For this purpose, a complete system of equations related to all equilibria in the solutions was solved using Maple6 (Waterloo Maple Software and University of Waterloo).

The morphology of the deposited films was studied by scanning electron microscopy (SEM) using a Zeiss MERLIN field-emission SEM at 5 keV. Their chemical composition was determined with an energy dispersive X-ray spectroscopy (EDX) analysis tool attached to the SEM at an acceleration voltage of 20 keV.

The mechanical properties of the Fe-Ga films were studied by nanoindentation. The indentations were performed on a Nanoindenter NHT^2 from Anton Paar equipped with a Berkovich pyramidal-shaped diamond tip under load-control mode. An array of 50 indentations was performed at the top surface of the films. The nanoindentation function consisted of a loading segment of 30 s, followed by a load holding segment of 10 s and an unloading segment of 30 s. The maximum applied load was set to 1 mN to avoid the influence from the substrate. The reduced elastic modulus (E_r) and hardness (H) were derived from the initial part of the unloading–displacement curve by applying the method of Oliver and Pharr. The plasticity index (W_{pl}/W_{tot}) was calculated as a ratio between plastic and total (plastic + elastic) energies during nanoindentation. The plastic energy (W_{pl}) was derived as the area between loading and unloading curves, while the total energy (W_{tot}) was calculated as the area between the loading curve and the displacement axis. From the obtained nanomechanical data, the porosity degree in the Fe-Ga films was estimated using Eq. (3):

$$P = 1 - \left(\frac{E_{porous}}{E_{bulk}}\right)^{1/n} \quad (3)$$

where P is the porosity degree, E_{porous} is the experimentally obtained reduced elastic modulus of the films, E_{bulk} is the elastic modulus of the fully dense material, and n is a density exponent that depends on the deformation mechanism of the cell ($n \approx 2$ for a material with an open cell porosity) [27]. E_{bulk} of Fe-Ga films was determined using the rule of mixtures for isostrain conditions (Eq.4):

$$E_{bulk} = fE_{Fe} + (1-f)E_{Ga} \quad (4)$$

where f is the atomic fraction of Fe in the deposit, and E_{Fe} and E_{Ga} are the elastic moduli of bulk Fe and Ga, respectively. All the extracted parameters were statistically treated, and average values are reported.

The magnetic properties of the Fe-Ga films were studied at room temperature using a VSM from MicroSense (LOT-Quantum Design). Hysteresis loops were recorded along the in-plane (with the substrate) and the out-of-plane directions with a maximum applied field of ± 20 kOe. For proper normalization of the hysteresis loops, the films were digested in aqua regia. The resulting solutions were analyzed by inductively coupled plasma mass spectrometry (ICP-MS) in a NexION350D spectrometer.

To study the structural and magnetostrictive properties of templated and non-templated Fe-Ga films, XRD patterns were acquired on a Philips X'Pert diffractometer using Cu Kα radiation in θ-2θ configuration. A constant magnetic field was applied in-situ and along the out-of-plane direction of the films using a NdFeB permanent magnet (Ø = 2 cm, 4000 Oe) placed inside the diffractometer. Fe-Ga samples with an area of 0.5 cm × 0.5 cm were placed on top and at the center of the permanent magnet and the *xyz* position of the sample in the XRD diffractometer was kept the same for the measurements without and with the magnetic field. Variations in structural parameters caused by the magnetic field were evaluated by Rietveld refinement using the 'Materials Analysis Using Diffraction' (MAUD) software.

3. Results and discussion

3.1. Fe-Ga co-deposition mechanism

Electrodeposition of Fe-Ga alloys is relatively difficult due to the high tendency of both metal precursor ions to hydrolyze in aqueous solutions. Electrodeposited Fe-Ga alloys are prone to passivate or even incorporate oxygen [28] which may alter the mechanical and magnetic performance of the films. Understanding the bath chemistry is a crucial step towards the optimization of the electrolyte performance. For this purpose, the distribution of various hydroxo- and organometallic species in the electrolyte was primarily estimated.

Fig. 2**a** provides the calculated mole fractions of Ga(III) containing species vs. pH in an aqueous $Ga_2(SO_4)_3$ solution. As it can be seen, Ga(III) ions form various mono- and polynuclear hydroxo-species over the entire range of pH. The distribution of various Fe^{2+} hydroxo-species is shown in Supporting **Figure S1**. However, the species distribution changes in the presence of the complexing agent used to stabilize the electrolyte (i.e., citrate) due to the reduction of the concentration of "free" Fe^{2+} and Ga^{3+} ions. Fig. 2**b** shows the calculated species distribution in the citrate electrolyte utilized in this work to deposit Fe-Ga films. The addition of the complexing agent to the bath significantly shifts equilibria towards the formation of complex compounds with citrate at pH > 2.5. The reduction of metal-containing species on the electrode gives rise to the respective shifts in the different chemical equilibria built in the electrolyte which involve complexes, ligands, hydronium ions, etc. Keeping this in mind, all processes in the systems under consideration should proceed through, at least, two

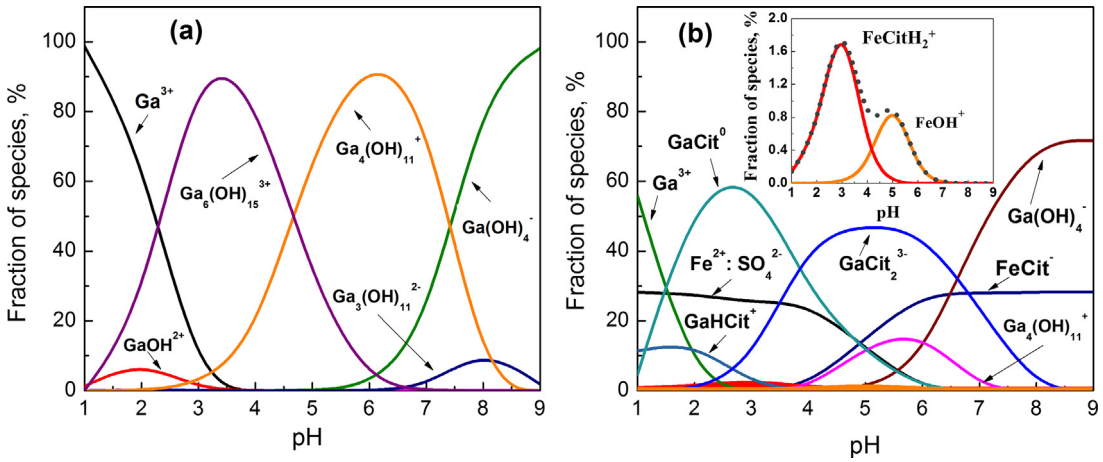

Fig. 2. Calculated fraction of (a) Ga(III) hydroxo-complexes in water, and (b) Fe(II) and Ga(III) species at the following total concentrations of electrolyte constituents: $[C_6H_8O_7]$ = 0.065 M, [Fe(II)] = 0.015 M and [Ga(III)] = 0.038 M. In panel (b), "Cit" stands for the citrate anion $C_6H_5O_7^{3-}$; dotted line represents the sum of equilibrium concentrations $[FeCitH_2^+]$ + $[FeOH^+]$. Equilibrium reactions and their constants used for the calculation are given in Table S1.

steps: a chemical step followed by an electrochemical one (charge transfer reaction), in other words, a certain chemical process generates the particle (i.e., the electrically active complex, EAC) that further takes part in the charge transfer. Although there is no thermodynamic limitation on the EAC composition (the same equilibrium potential is attributed to any charge transfer process), single electrically active species can be often defined, whereas all kinds of species participate in mass-transfer to the electrode. It is assumed in this case that these species supply the total current in the system, and the complex predominating in the solution does not need to be electrically active. Kinetic factors and the activation energy are responsible for the electrochemical activity of the complexes [29]. In addition, the electroreduction of Fe(II) and Ga(III) compounds to metallic state on the electrode involves multi-electron charge transfer reactions. This implies an intricate electroreduction mechanism involving a sequence of intermediate stages preferentially consisting of a single-electron transfer step and formation of adsorbed species. In the case of Fe(II) electroreduction from acidic solutions, three adsorbed species should at least be considered, and the corresponding intermediates must contain the OH^- anion in their structure [30]. According to the model of Bocris el al. [31,32] the intermediate in Fe(II) electroreduction from non-complexed solution is $Fe(OH)^+$. However, not only $Fe(OH)^+$ but also $Fe(HCitH_2)^+$, are present in the citrate solution used in our study (see Fig. 2**b**). Thus, the electroreduction mechanism involves formation of adsorbed zero-charged species followed by the single-electron transfer electrochemical reaction, and the electroreduction to Fe^0 during a slow (rate determining) subsequent stage, as follows:

$$FeL^+ + e^- \rightarrow Fe(I)L_{ads} \quad (5)$$

$$Fe(I)L_{ads} + e^- \rightarrow Fe + L^- \quad (6)$$

where L is either OH^-, or $CitH_2^-$ species.

The calculated partial current densities for both Fe(II) and Ga (III) electroreduction are presented in Fig. 3**a**. As it can be seen, the partial current density for Fe(II) electroreduction decreases significantly with increasing pH, which correlates well with a decrease in the sum of equilibrium concentrations $[FeCitH_2^+]$ + $[FeOH^+]$. This reveals that both these species act as EAC in Fe(II) electroreduction.

Investigations into gallium electroreduction mechanism are elusive. Nonetheless, in an analogous manner to Fe(II), a similar mechanism can be assumed for Ga(III) electroreduction. A positively charged Ga(III) specie, i.e., $Ga_4(OH)_{11}^+$ is presumed to act as EAC, therefore the electroreduction mechanism involves the following relatively slow formation of adsorbed particle:

$$Ga_4(OH)_{11}^+ + e \rightarrow Ga_4(OH)_{11,ads} \quad (7)$$

As it is seen from Fig. 3**a**, the partial current densities for Ga(III) slightly increase with an increase in pH. The different effect of pH on partial current densities for Fe(II) and Ga(III) electroreduction results in an increase of the Ga content in the alloys with increase in pH.

Electrodeposition conditions were first optimized for the non-templated Fe-Ga films. Fig. 3**b** shows the Ga content determined by both EDX and ICP-MS in films obtained by electrodeposition onto rigid Si/Au substrates. As it can be observed, Ga content in the deposit increases with pH for a fixed deposition potential, in accordance with the proposed co-deposition mechanism. The alloys are iron-rich because of the more positive Nernst potential of Fe in the studied electrolyte i.e., $E_{Fe^{2+}/Fe} = -0.51V$ vs. $E_{Ga^{3+}/Ga} = -0.67V$ at pH 3. Remarkably, the experimental results suggest that below this value, i.e., for pH < 3, only Fe (Ga-free) deposits can be obtained. An increase in cathodic polarization also leads to an increased Ga content in the deposits, that can reach up to 40 at.% under the investigated conditions.

3.2. Morphological characterization

The morphology of the non-templated Fe-Ga films changes significantly with the Ga content, Fig. 4**a-d.** Multifaceted grains with some intragrain nanoporosity particularly visible for 2–20 at.% Ga films (as it is indicated with the white arrows) is observed. This nanoporosity probably originates from the highly distorted columnar growth promoted by accompanying hydrogen evolution, as it can be observed in the cross-section SEM image in Fig. 4**g** (the white arrows point to large pores). A controllable degree of porosity in Fe-Ga films was achieved using colloidal crystal-templated substrates. Fig. 4**e,f** shows the representative SEM images of the top surface of the templated Fe-Ga films with varying Ga content, i.e. 20 and 33 at.% respectively. As expected, the pore diameter (~400 nm) matches the diameter of the latex spheres. A multilayer structure with an open-cell porosity and pore wall width of about 50–100 nm can be directly observed from the micrographs. Fig. 4**h** shows the fracture surface of templated Fe-Ga film having 20 at.%

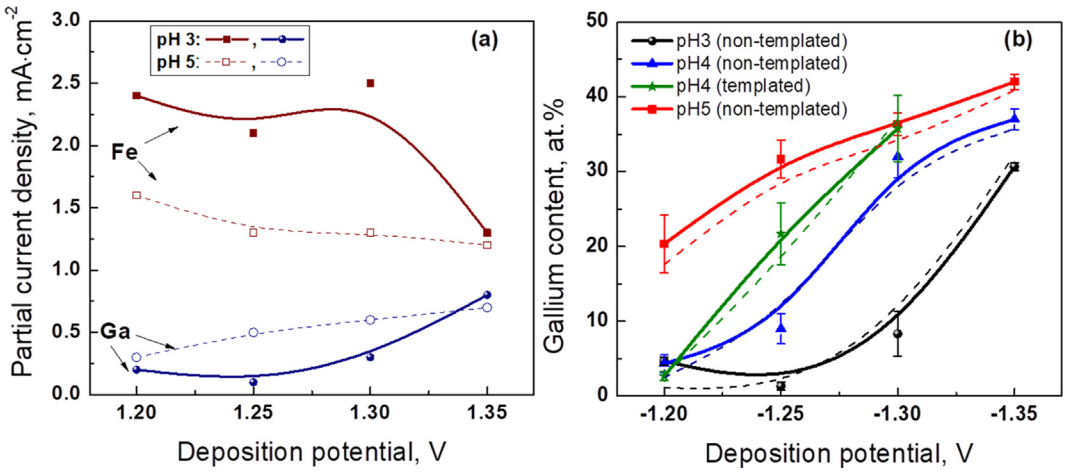

Fig. 3. (a) Partial current densities for Fe and Ga electrodeposition at various pH and potentials, and (b) composition of electrodeposited Fe-Ga alloys as a function of deposition potential and pH of electrolyte. Solid lines represent the composition obtained by EDX analysis and the dashed lines show the composition determined by ICP-MS analysis.

Ga in composition with macropores homogeneously distributed along the film thickness.

Remarkably, the composition of templated Fe-Ga alloys is different from the non-templated layers (i.e., films directly electrodeposited onto metallized Si substrates) produced under the same conditions (Fig. 3**b**), i.e., more Ga is incorporated when deposition occurs at the narrow regions between the close-packed spheres as compared to flat surfaces. This can be due to the hindered Fe species diffusion through the cavities that favors preferential Ga deposition [33]. In addition, the alkalization of the near-electrode surface can be more pronounced in the case of templated substrates, thus favoring the formation of Ga hydroxo-species that presumably facilitate Ga deposition as compared to citrate molecules (Fig. 2**b**). It is also worth mentioning that the Fe-Ga films normally contain up to 10 at.% of oxygen on the top surface, independently of the applied electrodeposition conditions (**Figure S2**). Nevertheless, EDX analysis on the cross-section of the films evidenced that there is only < 5 at.% in the interior of the layers. This means that the films undergo superficial surface oxidation after fabrication, while inclusion of oxides and hydroxides during electrodeposition is not promoted.

3.3. Mechanical properties

The influence of both porosity and chemical composition of electrodeposited Fe-Ga films on their mechanical properties was investigated by nanoindentation. Dense film of Fe-Ga with 20 at.%Ga produced by sputtering was used as a reference material. Fig. 5**a** shows representative load–displacement curves from where various nanomechanical parameters were extracted after applying the method of Oliver-Pharr [34]. It can be observed that the maximum and final penetration, the slope at the beginning of the unloading segment and the areas under the loading and/or unloading curves vary depending on the composition and the degree of porosity of the films. Indeed, concerning the reduced Young's modulus (E_r), for samples with similar compositions (i.e., 20 at.%), the dense sample has the highest value, while E_r decreases significantly for the non-templated and even further for the templated electrodeposited Fe-Ga layers (Fig. 5**b**, **Table S2**). Remarkably, the elastic modulus of the reference sample is very close to the bulk value estimated from the rule of mixtures (Eq. (4). taking E_{Fe} = 211 GPa, E_{Ga} = 9.6 GPa [35]), confirming that the sputtered Fe-Ga films are truly dense and virtually free of porosity. The correlation between elastic modulus and porosity degree is well documented and it is given by Eq. (3), from where the porosity of the specimens can be calculated based on the measured mechanical properties [27,36]. The obtained values of porosity are reported in **Table S2**. The results suggest that the non-templated films contain about 10–20% fraction of pores. This correlates well with the morphological features revealed in Fig. 4. As the Ga content in the films increases, the shape of the grains becomes more regular allowing them to pack closer. This contributes to a reduction in porosity in the films.

The porosity degree in templated Fe-Ga films reaches up to 35% according to the nanoindentation data. Nevertheless, according to the literature, the porosity in colloidal templated films can reach up to 65%, as it was demonstrated by ellipsometry measurements in electrodeposited Fe-Cu films templated with 200 nm PS spheres [23]. A priori, one may assume that the porosity degree in the templated deposits is directly dictated by the size of the spheres (which are much larger than the size of the pores produced during electrodeposition). This would give the same porosity level to all templated films, independently of their composition. However, the porosity degree for the templated samples increases with the Ga content (contrary to what happens when depositing onto a flat surface). This is most likely caused by the inherent "second-order" porosity in Fe-Ga attributed to the Fe-Ga grain structure, i.e., larger grains of Ga-rich alloy are more difficult to accommodate in narrow spaces between the PS spheres, thus producing more voids, as compared to the smaller grains of more Fe-rich deposits. As a result, colloidal templated films show dual or hierarchical porosity, i.e., macropores caused by the PS spheres and nanopores in the pore walls.

Yet, the porosity degree obtained from nanoindentation data is likely underestimated due to the compaction of pores that occurs under the indenter tip during loading. This can be inferred from the shape of characteristic load–displacement curves of the highly porous templated samples where a pronounced "flattening" of the loading segment is observed at low forces. That is, as the applied load is increasing slowly the indentation depth changes significantly due to the densification of the porous microstructure [37]. Supporting **Figure S3** shows an indentation imprint obtained at 20 mN and clearly evidences the pore compaction. Note that even at 1 mN several pores of the templated Fe-Ga films are embraced since the indentation contact area (estimated by the model of Oliver and Pharr) is around 0.6–0.8 μm^2 for the templated sample (thus larger than the size of the macropores).

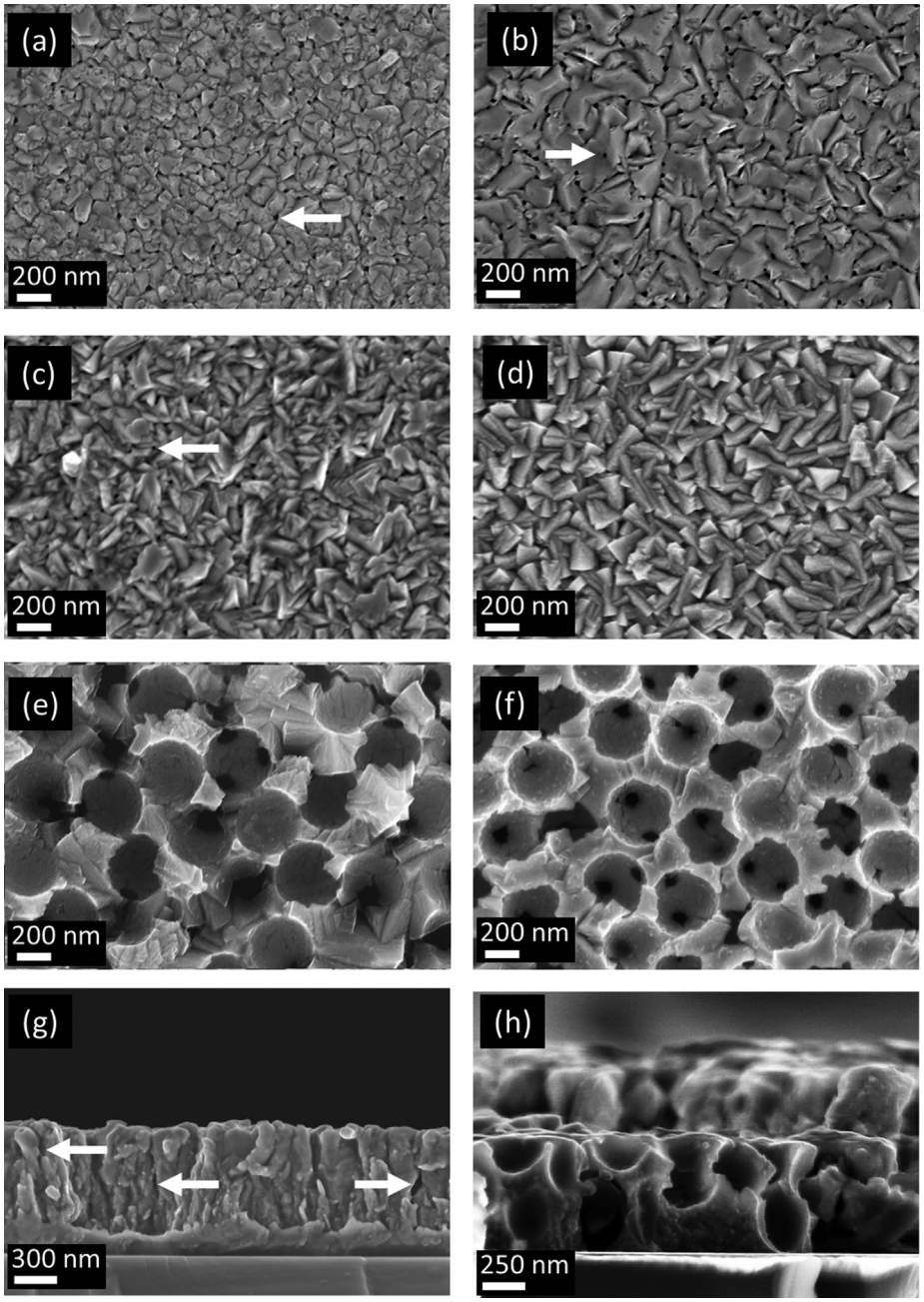

Fig. 4. Representative SEM images of the Fe-Ga films. Panels a-d show the top surface of the non-templated films: (a) 2 at.% Ga; (b) 15 at.% Ga; (c) 20 at.% Ga; and (d) 33 at.% Ga. Panels e,f show the top surface of the templated films: (e) 20 at.% Ga; and (f) 33 at.% Ga. Panels g,h show the fracture surfaces (cross-sections) of the Fe-Ga films with 20 at. % Ga: (g) non-templated; (h) templated. White arrows indicate the pores.

The presence of pores in electrodeposited Fe-Ga films is also the most likely factor responsible for the observed reduction in hardness of non-templated and templated films as compared to the fully dense reference sample. Hardness is directly related to the yield stress, which, in turn, is directly proportional to the porosity degree [36]. Furthermore, taking into account that the macroscopic hardness of Ga is generally smaller than that of Fe (by a reported factor of at least 3.5 [35]), the decrease in hardness for larger Ga contents (**Table S2**) can be understood again based on the rule of mixtures argument. Grain size can also play a role in the reduction of both, hardness and Young's modulus of the alloys, as it is well-documented in the literature [38]. Nevertheless, in the case of highly porous films this effect is most likely negligible as compared to the other two (i.e., porosity degree and Fe:Ga ratio in the films) [39].

Finally, the elastic–plastic response of the films can be also studied from the nanoindentation data. The load–displacement curves of electrodeposited templated and non-templated Fe-Ga films (Fig. 5**a**) feature so-called "pop-in" events, i.e., sudden bursts during the loading of the indenter onto the sample. Generally, in fully dense polycrystalline materials such plastic instability may arise from the dislocation nucleation, formation of stacking faults, cracks, etc. (not noticed in the sputtered reference Fe-Ga prepared in this work) [40]. In the case of porous Fe-Ga films the pop-in events most likely caused by the abrupt densification of the pores or their collapse due to the brittle nature of the material [41]. The

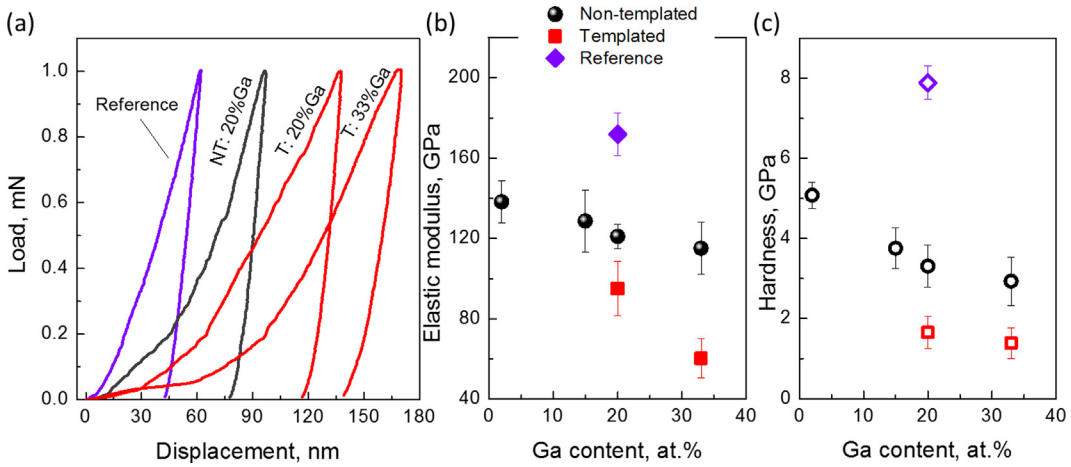

Fig. 5. Mechanical properties of Fe-Ga alloys at 1 mN: (a) representative load–displacement curves for the reference (dense, sputtered) Fe-Ga sample, non-templated "NT" and templated "T" electrodeposited Fe-Ga films; (b) reduced Young's modulus of the Fe-Ga films as a function of the Ga content; (c) hardness of the investigated Fe-Ga films. The legend in the panel (b) applies also to the panel (c), where the same but empty symbols are used instead of filled symbols.

elastic strain to failure, H/E_r, and the plasticity index, W_{pl}/W_{tot}, were also derived (see experimental section for details). The former indicates how much the material can be elongated to failure, and the later shows the ability of the material to absorb plastic deformations. The results presented in **Table S2** indicate that for a given composition (i.e., 20 at.%), the plastic energy is larger as the porosity degree increases. Interestingly, there is a linear correlation between the two above-mentioned parameters [34,42], which is also confirmed for the studied Fe-Ga system (see **Figure S3**).

3.4. Magnetic properties

The magnetic properties of the dense and porous Fe-Ga films having 20 and ~ 30 at.% of Ga (composition corresponding to maxima in magnetostriction) were studied by VSM. Fig. 6 and **Figure S5** show magnetization hysteresis loops of the Fe-Ga films with 20 at.% of Ga but different porosity degree. The hysteresis loops of the films with 33 at.% Ga are shown in Supporting **Figure S6**. In all cases, the remanence-to-saturation magnetization ratio, M_r/M_s, measured along the out-of-plane direction, is lower than for the in-plane direction (Table 1), which indicates the magnetic easy axis lies in the plane of the films (in spite of porosity). The overall shape of the in-plane hysteresis loops is squarer, which means the films become magnetically saturated at lower magnetic fields. In the porous samples the loops recorded in the out-of-plane direction become less tilted with respect to in-plane, i.e., the difference in M_r/M_s in-plane and out-of-plane directions decreases. Such behavior indicates that the hysteresis behavior of the denser Fe-Ga films is governed by the shape anisotropy but this effect is partially lost in the porous samples. This also leads to a reduction of the out-of-plane saturation field in the templated samples (Table 1). It is worth mentioning that at magnetic saturation, the magnetostrictive strain reaches a maximum, such as all the magnetic domains become aligned with the magnetic field [43]. Therefore, based on these data it can be assumed that in porous Fe-Ga samples the maximum magnetostriction along the out-of-plane direction can be induced at lower fields as compared to the fully dense, or non-templated samples.

Remarkably, contrary to the fully dense reference (sputtered) sample, the hysteresis loops of both non-templated and templated (electrodeposited) films recorded along out-of-plane show a widening when approaching coercive field. Such 'out-of-plane component' has been previously observed in various Fe-Ga film systems, regardless of the growth method, although to a different extent, that makes it difficult to establish a direct correlation with the structural and compositional characteristics of the films [18,44]. Very recently, it has been demonstrated that the appearance of such out-of-plane magnetic component in Fe-Ga alloys

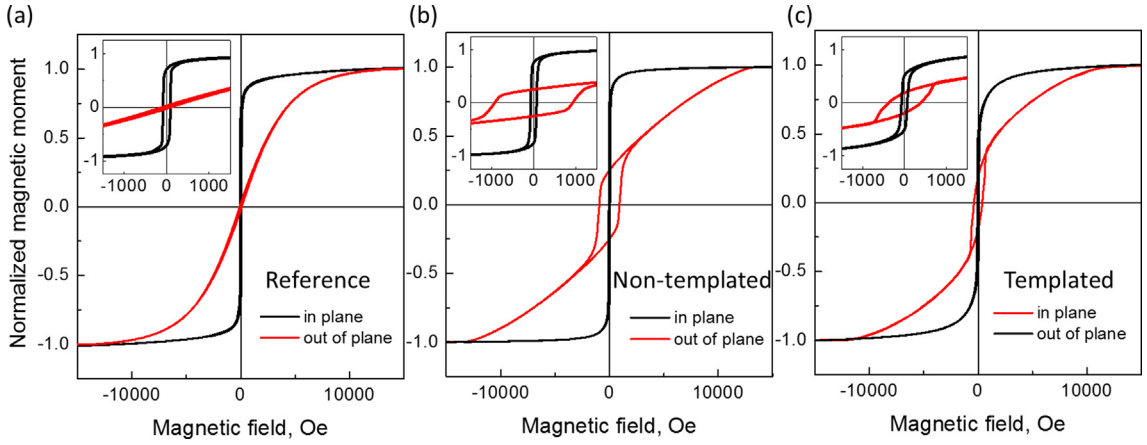

Fig. 6. In plane and out of plane hysteresis loops for Fe-Ga layers with 20 at.% of Ga: (a) reference – fully dense, (b) non-templated – nanoporous Fe-Ga, and (c) templated film – macroporous Fe-Ga. Insets show the magnified central area of the corresponding loops.

Table 1
Summary of the magnetic properties of the Fe-Ga films obtained from VSM measurements. "NT" – non-templated, "T" – templated.

Sample	Ga, at.%	Saturation magnetization, emu/g	Saturation field ⊥, kOe	Coercivity, Oe		Remanence-to-saturation magnetization ratio M_r/M_s		
				∥	⊥	∥	⊥	Δ(∥-⊥)
Reference	20	176	14.0	86	86	0.68	0.02	0.66
NT	20	187	13.7	69	926	0.74	0.24	0.50
NT	33	100	12.5	94	186	0.56	0.03	0.53
T	20	178	12.3	70	365	0.51	0.18	0.33
T	33	112	11.0	70	86	0.35	0.02	0.33

can be due to the presence of several magnetic phases with competing anisotropies [45].

An addition of Ga to Fe leads to a reduction of saturation magnetization (M_s), as it can be expected from the dilution of magnetic Fe (M_s(Fe) = 217 emu/g [46]) by non-magnetic Ga atoms. Nevertheless, the dependence of M_s follows a linear trend with the composition only up to ~ 20 at.% of Ga [47]. Above this concentration, the magnetization versus Ga content changes slope and drastically decreases due to the change in structural ordering of the Ga-rich alloys [48]. This explains the considerable variation of M_S between the samples with 20 and 33 Ga at. %.

3.5. Structural and magnetostrictive properties

Essentially, the conversion between the mechanical and magnetic energies in Fe-Ga is realized through magnetostriction. In this work, structural characterization and assessment of magnetostriction in the Fe-Ga films was performed by XRD. Fig. 7**a** shows the XRD pattern corresponding to the templated (macroporous) Fe-Ga film with ~ 20 at.% of Ga, while the XRD pattern of the non-templated film with the same composition is shown in Supporting **Figure S7a**. The patterns were recorded in a relatively narrow region capturing the strongest Fe-Ga reflection, that is (1 1 0) [9,25], and the substrate (Au (1 1 1)) peak that served as a reference for determination of magnetostriction in subsequent experiments.

Iron and gallium are highly miscible (Ga solubility in body-centered cubic (bcc)-Fe is 47.5 at.%) and may form both solid solutions and intermetallic compounds, namely: Fe_3Ga, Fe_6Ga_5, Fe_3Ga_4, and $FeGa_3$ (with increasing Ga content) [49]. Among them, a disordered bcc α-Fe(Ga) solid solution (or A2 phase) is typically found in electrodeposited films [2,9,50,51], although the formation α-Fe_3Ga phase in electrodeposits has been also reported [28]. Increasing the Ga content in the films may lead to the appearance of several ordered phases (coherent with the parent A2 cubic structure), such as cubic B2, bcc-D03, or fcc-L12. This is observed in films prepared by physical methods, e.g., arc melting or sputtering [52–54]. Sometimes, the ordered and disordered phases coexist (even in non-annealed samples [55]) and so, the understanding of the structural properties of the films becomes more complex [45].

In Fig. 7**a**, two peaks at around 44-45° can be observed. The two peaks can be attributed to the (1 1 0) reflection of Fe(Ga) solid solutions, with dissimilar lattice parameters. No peaks of oxides or Fe-Ga intermetallic compounds are present (in a wide 2θ range). For simplicity, the peak at lower 2θ angle is denoted as "A" and the second peak separated by 0.6° from "A" is symbolized as "B". Since Ga has a slightly larger atomic radius than Fe, the random substitution of Fe atoms by Ga when forming a solid solution causes an increase in the lattice parameter and shifts the peaks' position towards lower 2θ angles. Thus, phase B is likely to have less Ga, as compared to phase A. The Vegard's law can be used to estimate the composition of each phase. To obtain the cell parameters of "A" and "B", the patterns were refined by Rietveld method using MAUD software. Based on values reported in Ref. [50], the cell parameter of the phase "A" corresponds to approximately 22 at.% of Ga, while

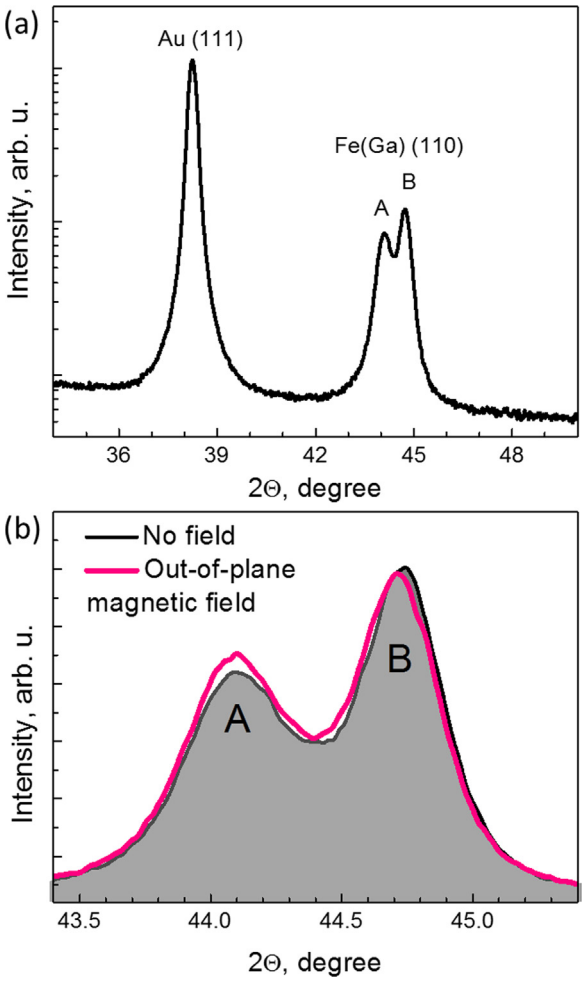

Fig. 7. X-ray diffraction patterns of templated Fe-Ga alloy with 20 at.% Ga: (a) wide 2θ range capturing the seed-layer (gold) peak used as a reference recorded with no magnetic field applied, and (b) narrow 2θ range showing the two peaks of (1 1 0)-Fe(Ga) solid solution with no field and with an out of plane magnetic field of 0.4 T.

the phase "B" is more Fe-rich having ~ 12 at.% of Ga. This gives an average of 17 at.% of Ga in the templated film, in accordance with ICP-MS results (Fig. 3). It is worth mentioning that such phase separation is typically not observed in as-prepared Fe-Ga films, and so far, remains not fully understood. The presence of two clear peaks with well distinguished cell parameters implies that the phase separation is not attributed to the compositional gradients (that may develop in some cases due to the local variations in pH near the electrode [28]). Remarkably, that the non-templated Fe-Ga films also exhibit a double (1 1 0)-peak (**Figure S7a**), and therefore, the observed effect is reproducible regardless of the templating method. The effects of substrate could not explain the double peak because the substrate itself does not diffract in this angular range.

In addition to having two A2 solid solutions, the splitting of the peaks could also be due to the formation of ordered phases within the A2 matrix, in accordance with reported metastable Fe-Ga phase diagrams [56,57]. Such metastability could be reached during electrodeposition since the potential applied to the electrode drives the electrochemical system far from the situation predicted by the equilibrium phase diagram [58–63]. Indeed, according to the phase diagram reported in Ref. [57], the phase "A" may contain D03 clusters (22 at.% Ga) and phase "B" - A2 structure (12 at.% Ga). Interestingly, the splitting of the Fe(Ga) peaks has been also shown in Ref. [21], although the interpretation remained elusive. Most likely phase separation occurs at the nanoscale and is probably governed by the intricate adsorption and nucleation mechanisms occurring during electrodeposition.

To assess the magnetostriction in templated and non-templated Fe-Ga films, an external magnetic field was applied in-situ while recording the XRD patterns. Theoretical works involving grain averaging theory for modelling heterogeneous materials (Green's function) have shown that the magnetostriction effect is sensitive not only to the single crystal constants but also to microstructure, such as crystal anisotropy and porosity [64,65]. Formally, the macroscopic behavior of a polycrystal can be quantitatively assessed using so-called "effective medium expression" (or effective medium approximation) that accounts for the effects of crystal constants, microstructural features, and applied fields. Thus, numerical simulation showed that the magnetostriction of a polycrystal can either decrease if $|\lambda_{111}| > |\lambda_{100}|$, in e.g. Fe or Terfenol-D, or increase if the $|\lambda_{111}| < |\lambda_{100}|$, as in the case of Ni and Fe-Co [64]. It should be noted that the experimental determination of magnetostriction in porous materials remains challenging. Most of the methods to estimate the magnetostriction constant rely on bending the films using an underlying substrate (e.g., standard strain gauge method). However, in case of non-constrained geometries, like in highly porous films where there is a limited contact between the layer and the substrate, these methods are not very reliable, basically because the deformations induced by magnetic field are not effectively transferred to the substrate and the induced deformations can be accommodated through the empty space in the pores. Thus, standard magnetostriction measurements based on the macroscopic specimen deformation cannot be applied to study the here-prepared porous materials. Alternatively, XRD with magnetic field measurements can provide information about the "internal magnetostriction", i.e., magnetic field induced crystallographic deformation within each unit cell [66,67]. Upon application of a magnetic field, the reorientation of magnetic domains can lead to an expansion or contraction of the lattice, which can cause a shift of the corresponding XRD peaks [67–70].

Indeed, it has been observed that under an external magnetic field both (1 1 0)-Fe(Ga) peaks are shifted towards lower 2θ angles, as depicted in Fig. 7**b**. The magnetostriction of Au is negligible and therefore the position of the peak can serve as a reference (**Figure S7**). The obtained patterns were analyzed using Rietveld refinement from where the magnetic-field induced changes in (1 1 0)-Fe(Ga) cell parameter were calculated as a percent fraction from the initial value. As expected, the cell parameter of the reference, fully constrained (dense) sample almost does not change with the external magnetic field (i.e., an increase in cell parameter from initial state is ~ 0.003%). This result could be anticipated due to the clamping with the rigid support (metallized Si) that hinders the generation of strain. Contrarily, the cell parameter of the non-templated Fe-Ga film increases by approximately 0.033% for phase "A" and 0.012% for phase "B". In this sample, upon application of magnetic field, the residual nanoporosity in between the Fe-Ga grains allows the material to deform at a certain distance from the substrate, thus significantly reducing the clamping effect through the development of strain gradients along the vertical direction [9]. The templated Fe-Ga films show an even larger magnetic-field induced variation of the cell parameter, i.e., an increase by 0.033% for phase "A" and by 0.045% for phase "B". The increase in the cell parameter is accompanied by an increase in the microstrains due to cell distortion. These results are in accordance with previous theoretical works from which an enhanced magnetostriction with porosity in materials with $\lambda_{111} < \lambda_{100}$ (characteristic for Fe-Ga alloys [26]) was inferred [64]. Nevertheless, the complexity of the system does not allow to easily discern between different possible magnetostriction contributions (i.e., "internal magnetostriction" due to dipole–dipole interactions, versus "volume magnetostriction").

4. Conclusions

Fe-Ga alloys were electrodeposited from citrate electrolyte onto rigid metalized silicon substrates. The co-deposition mechanism of Fe-Ga alloys is discussed based on strong interdependences from electrochemically active complexes, such as $FeCitH_2^+$, $FeOH^+$ and $Ga_4(OH)_{11}^+$. The different influence of pH on partial current densities for Fe(II) and Ga(III) electroreduction correlates well with the concentrations of positive single-charged species. This leads to the possibility of tuning the composition of the films (in the range 2 – 40 at.% of Ga) by varying the pH value of the electrolyte and the electrodeposition potential. Alloys with different porosity levels, i.e., nanoporous vs. macroporous layers, were prepared in our work. The films directly grown on silicon exhibited a certain degree of inherent nanoporosity within the pore walls endowed by hydrogen coevolution, and macroporous films were produced by electrodeposition through colloidal crystal templates. The induced porosity significantly reduces the Young's modulus and the hardness of electrodeposited Fe-Ga films, as compared to fully dense sputtered layers. Increasing the Ga content from a few at.% to 30 at.% causes the hardness to decrease from 5 GPa to ~ 1 GPa (in the case of Ga-rich templated film), respectively. However, the presence of pores increases the plasticity index, which is as important parameter indicative of the film's ability to accommodate plastic deformations. In terms of magnetic properties, addition of Ga to Fe decreases the saturation magnetization, although the dependence does not follow a linear trend with the overall compositional range. The shape anisotropy is partially lost in the porous samples and the out-of-plane saturation field is decreased, suggesting that, along this direction, the maximum magnetostriction can be achieved at lower magnetic fields as compared to the fully dense films. Finally, the magnetic-field induced changes in lattice constants of the non-templated (nanoporous) and templated (macroporous) Fe-Ga films were evaluated by XRD. The results demonstrate that under the action of external magnetic field the macroporous Fe-Ga films exhibit a larger crystal deformation, as compared to nanoporous and fully dense counterparts, i.e., the cell parameter is increased by 0.033 – 0.045%. Thus, the reduction of lateral constraints due to porosity minimizes the clamping effect with rigid substrates and allows for strain gradients. In addition, the pores could accommodate second-phase materials, thus opening new possibilities for the design of various composite materials, such as exchanged coupled systems or magnetoelectric heterostructures integrated on silicon.

Declaration of Competing Interest

The authors declare that they have no known competing financial interests or personal relationships that could have appeared to influence the work reported in this paper.

Acknowledgements

This work has received funding from the European Union's Horizon 2020 research and innovation programme under the Marie Sklodowska-Curie grant agreement N° 892661– MAGNUS and partially from N° 778357- SMARTELECTRODES. Financial support by the European Research Council (SPIN-PORICS 2014-Consolidator Grant (N° 648454) and MAGIC-SWITCH 2019-Proof of Concept Grant (N° 875018)), the Spanish Government (MAT2017-86357-C3-1-R and associated FEDER) and the Generalitat de Catalunya (2017-SGR-292) is also acknowledged.

Data availability

The raw/processed data required to reproduce these findings cannot be shared at this time as the data also forms part of an ongoing study. The data that support the findings of this study are available from the corresponding authors on request.

Appendix A. Supplementary data

Supplementary data to this article can be found online at https://doi.org/10.1016/j.matdes.2021.109915.

References

[1] A. Rodzinski, R. Guduru, P. Liang, A. Hadjikhani, T. Stewart, E. Stimphil, C. Runowicz, R. Cote, N. Altman, R. Datar, S. Khizroev, Targeted and controlled anticancer drug delivery and release with magnetoelectric nanoparticles, Sci. Rep. 6 (2016) 20867.

[2] X.Z. Chen, M. Hoop, N. Shamsudhin, T. Huang, B. Özkale, Q. Li, E. Siringil, F. Mushtaq, L. Di Tizio, B.J. Nelson, S. Pané, Hybrid Magnetoelectric Nanowires for Nanorobotic Applications: Fabrication, Magnetoelectric Coupling, and Magnetically Assisted In Vitro Targeted Drug Delivery, Adv. Mater. 29 (2017) 1605458, https://doi.org/10.1002/adma.201605458.

[3] V. Annapureddy, H. Palneedi, G.T. Hwang, M. Peddigari, D.Y. Jeong, W.H. Yoon, K.H. Kim, J. Ryu, Magnetic energy harvesting with magnetoelectrics: An emerging technology for self-powered autonomous systems, Sustain. Energy Fuels. 1 (2017) 2039–2052, https://doi.org/10.1039/c7se00403f.

[4] F. Mushtaq, X. Chen, H. Torlakcik, C. Steuer, M. Hoop, E.C. Siringil, X. Marti, G. Limburg, P. Stipp, B.J. Nelson, S. Pané, Magnetoelectrically Driven Catalytic Degradation of Organics, Adv. Mater. 31 (2019) 1901378, https://doi.org/10.1002/adma.201901378.

[5] B.J.H. Stadler, M. Reddy, R. Basantkumar, P. McGary, E. Estrine, X. Huang, S.Y. Sung, L. Tan, J. Zou, M. Maqableh, D. Shore, T. Gage, J. Um, M. Hein, A. Sharma, Galfenol thin films and nanowires, Sensors (Switzerland). 18 (2018), https://doi.org/10.3390/s18082643.

[6] C. Vargas-Estevez, A. Blanquer, P. Dulal, R. Pérez del Real, M. Duch, E. Ibáñez, L. Barrios, G. Murillo, N. Torras, C. Nogués, B.J.H. Stadler, J.A. Plaza, J. Esteve, Study of Galfenol direct cytotoxicity and remote microactuation in cells, Biomaterials. 139 (2017) 67–74, https://doi.org/10.1016/j.biomaterials.2017.05.049.

[7] H. Wang, Y. Zheng, J. Liu, C. Jiang, Y. Li, In vitro corrosion properties and cytocompatibility of Fe-Ga alloys as potential biodegradable metallic materials, Mater. Sci. Eng. C. 71 (2017) 60–66, https://doi.org/10.1016/j.msec.2016.09.086.

[8] R.N. Torah, S.P. Beeby, N.M. White, Experimental investigation into the effect of substrate clamping on the piezoelectric behaviour of thick-film PZT elements, J. Phys. D. Appl. Phys. 37 (2004) 1074–1078, https://doi.org/10.1088/0022-3727/37/7/019.

[9] A. Nicolenco, A. Gómez, X.Z. Chen, E. Menéndez, J. Fornell, S. Pané, E. Pellicer, J. Sort, Strain gradient mediated magnetoelectricity in Fe-Ga/P(VDF-TrFE) multiferroic bilayers integrated on silicon, Appl. Mater. Today. 19 (2020), https://doi.org/10.1016/j.apmt.2020.100579 100579.

[10] P. Zubko, G. Catalan, A.K. Tagantsev, Flexoelectric Effect in Solids, Annu. Rev. Mater. Res. 43 (2013) 387–421, https://doi.org/10.1146/annurev-matsci-071312-121634.

[11] A. Nicolenco, M. de h-Ora, C. Yun, J. MacManus-Driscoll, J. Sort, Strain-gradient effects in nanoscale-engineered magnetoelectric materials, APL Mater. 9 (2021) 20903. doi:10.1063/5.0037421.

[12] L. Jaouen, A. Renault, M. Deverge, Elastic and damping characterizations of acoustical porous materials: Available experimental methods and applications to a melamine foam, Appl. Acoust. 69 (2008) 1129–1140, https://doi.org/10.1016/j.apacoust.2007.11.008.

[13] G. Ryan, A. Pandit, D.P. Apatsidis, Fabrication methods of porous metals for use in orthopaedic applications, Biomaterials. 27 (2006) 2651–2670, https://doi.org/10.1016/j.biomaterials.2005.12.002.

[14] D. Chien, A.N. Buditama, L.T. Schelhas, H.Y. Kang, S. Robbennolt, J.P. Chang, S.H. Tolbert, Tuning magnetoelectric coupling using porosity in multiferroic nanocomposites of ALD-grown $Pb(Zr,Ti)O_3$ and templated mesoporous $CoFe_2O_4$, Appl. Phys. Lett. 109 (2016), https://doi.org/10.1063/1.4962536 112904.

[15] P. Martins, R. Gonçalves, A.C. Lopes, E. Venkata Ramana, S.K. Mendiratta, S. Lanceros-Mendez, Novel hybrid multifunctional magnetoelectric porous composite films, J. Magn. Magn. Mater. 396 (2015) 237–241, https://doi.org/10.1016/j.jmmm.2015.08.041.

[16] F. Mushtaq, H. Torlakcik, Q. Vallmajo-Martin, E.C. Siringil, J. Zhang, C. Röhrig, Y. Shen, Y. Yu, X.-Z. Chen, R. Müller, B.J. Nelson, S. Pané, Magnetoelectric 3D scaffolds for enhanced bone cell proliferation, Appl. Mater. Today. 16 (2019) 290–300, https://doi.org/10.1016/j.apmt.2019.06.004.

[17] T.E. Quickel, V.H. Le, T. Brezesinski, S.H. Tolbert, On the correlation between nanoscale structure and magnetic properties in ordered mesoporous cobalt ferrite ($CoFe_2O_4$) thin films, Nano Lett. 10 (2010) 2982–2988, https://doi.org/10.1021/nl1014266.

[18] E.C. Estrine, W.P. Robbins, M.M. Maqableh, B.J.H. Stadler, E.C. Estrine, W.P. Robbins, M.M. Maqableh, B.J.H. Stadler, Electrodeposition and characterization of magnetostrictive galfenol (FeGa) thin films for use in microelectromechanical systems, J. Appl. Phys. 113 (2013) 17A937, https://doi.org/10.1063/1.4799775.

[19] D. Cao, Z. Wang, L. Pan, H. Feng, X. Cheng, Z. Zhu, J. Wang, Q. Liu, G. Han, Controllable magnetic and magnetostrictive properties of FeGa films electrodeposited on curvature substrates, Appl. Phys. A Mater. Sci. Process. 122 (2016) 938, https://doi.org/10.1007/s00339-016-0468-y.

[20] M. Hein, J. Park, J.A. Cozzo, A. Flatau, B.J.H. Stadler, Electrodeposited Fe-Ga Alloy Films for Directly Coupled Noncontact Torque Sensing, IEEE Sens. J. 19 (2019) 6655–6661, https://doi.org/10.1109/JSEN.2019.2906062.

[21] P.D. McGary, K.S.M. Reddy, G.D. Haugstad, B.J.H. Stadler, Combinatorial Electrodeposition of Magnetostrictive $Fe_{1-x}Ga_x$, J. Electrochem. Soc. 157 (2010) D656–D665, https://doi.org/10.1149/1.3497355.

[22] C. Navarro-Senent, J. Fornell, E. Isarain-Chávez, A. Quintana, E. Menéndez, M. Foerster, L. Aballe, E. Weschke, J. Nogués, E. Pellicer, J. Sort, Large Magnetoelectric Effects in Electrodeposited Nanoporous Microdisks Driven by Effective Surface Charging and Magneto-Ionics, ACS Appl. Mater. Interfaces. 10 (2018) 44897–44905, https://doi.org/10.1021/acsami.8b17442.

[23] E. Dislaki, S. Robbennolt, M. Campoy-Quiles, J. Nogués, E. Pellicer, J. Sort, Coercivity Modulation in Fe–Cu Pseudo-Ordered Porous Thin Films Controlled by an Applied Voltage: A Sustainable, Energy-Efficient Approach to Magnetoelectrically Driven Materials, Adv. Sci. 5 (2018) 1800499, https://doi.org/10.1002/advs.201800499.

[24] A. Nicolenco, C. Navarro-Senent, J. Sort, Nanoporous Composites With Converse Magnetoelectric Effects for Energy-Efficient Applications, Ref. Modul. Mater. Sci. Mater. Eng. (2021), https://doi.org/10.1016/b978-0-12-803581-8.11870-3.

[25] E.C. Estrine, M. Hein, W.P. Robbins, B.J.H. Stadler, Composition and crystallinity in electrochemically deposited magnetostrictive galfenol (FeGa), J. Appl. Phys. 115 (2014) 17A918, https://doi.org/10.1063/1.4865318.

[26] J. Atulasimha, A.B. Flatau, A review of magnetostrictive iron-gallium alloys, Smart Mater. Struct. 20 (2011) 43001, https://doi.org/10.1088/0964-1726/20/4/043001.

[27] R. Domingo-Roca, D. Esqué-de los Ojos, M. Guerrero, E. Pellicer, M.D. Baró, S. Suriñach, J. Sort, Nanomechanical behavior of 3D porous metal-ceramic nanocomposite Bi/Bi2O3 films, Mater. Sci. Eng. A. 626 (2015) 150–158. doi:10.1016/j.msea.2014.12.042.

[28] D. Iselt, U. Gaitzsch, S. Oswald, S. Fähler, L. Schultz, H. Schlörb, Electrodeposition and characterization of $Fe_{80}Ga_{20}$ alloy films, Electrochim. Acta. 56 (2011) 5178–5183, https://doi.org/10.1016/j.electacta.2011.03.046.

[29] A. Survila, Electrochemistry of Metal Complexes: Applications from Electroplating to Oxide Layer Formation, Wiley-VCH, Weinheim, Germany, 2015.

[30] S.L. Díaz, J.A. Calderón, O.E. Barcia, O.R. Mattos, Electrodeposition of iron in sulphate solutions, Electrochim. Acta. 53 (2008) 7426–7435, https://doi.org/10.1016/j.electacta.2008.01.015.

[31] J.O.M. Bockris, D. Drazic, A.R. Despic, The electrode kinetics of the deposition and dissolution of iron, Electrochim. Acta. 4 (1961) 325–361, https://doi.org/10.1016/0013-4686(61)80026-1.

[32] W.C. Grande, J.B. Talbot, Electrodeposition of Thin Films of Nickel-Iron: II. Modeling, J. Electrochem. Soc. 140 (1993) 675–681, https://doi.org/10.1149/1.2056141.

[33] K.S.M. Reddy, E.C. Estrine, D.H. Lim, W.H. Smyrl, B.J.H. Stadler, Controlled electrochemical deposition of magnetostrictive $Fe_{1-x}Ga_x$ alloys, Electrochem. Commun. 18 (2012) 127–130, https://doi.org/10.1016/j.elecom.2012.02.039.

[34] W.C. Oliver, G.M. Pharr, Measurement of hardness and elastic modulus by instrumented indentation: Advances in understanding and refinements to methodology, J. Mater. Res. 19 (2004) 3–20, https://doi.org/10.1557/jmr.2004.19.1.3.

[35] F. Cardarelli, Materials Handbook, 3rd ed., Springer International Publishing, 2018. doi:10.1038/150195b0.

[36] E. Pellicer, S. Pané, V. Panagiotopoulou, S. Fusco, K.M. Sivaraman, S. Suriñach, M.D. Baró, B.J. Nelson, J. Sort, Localized electrochemical deposition of porous Cu-Ni microcolumns: Insights into the growth mechanisms and the mechanical performance, Int. J. Electrochem. Sci. 7 (2012) 4014–4029.

[37] Z. Chen, Nanoindentation of Macro-porous Materials for Elastic Modulus and Hardness Determination, in: T. Atul, S. Natarajan (Eds.), Appl. Nanoindentation Adv. Mater., 2017: pp. 135–156. doi:10.1002/9781119084501.ch6.
[38] G.Z. Yuliy, D. Gamburg, Theory and practice of metal electrodeposition, Springer (2011).
[39] K. Eiler, J. Fornell, C. Navarro-Senent, E. Pellicer, J. Sort, Tailoring magnetic and mechanical properties of mesoporous single-phase Ni-Pt films by electrodeposition, Nanoscale. 12 (2020) 7749–7758, https://doi.org/10.1039/c9nr10757f.
[40] F. Pöhl, Pop-in behavior and elastic-to-plastic transition of polycrystalline pure iron during sharp nanoindentation, Sci. Rep. 9 (2019) 15350, https://doi.org/10.1038/s41598-019-51644-5.
[41] V.A. Milyutin, I.V. Gervasieva, Application of the instrumented nanoindentation method ro evaluating the behavior of the mechanical properties of Fe-Ga alloys with increading gallium content, Diagnostics, Resour. Mech. Mater. Struct. 66 (2018) 90–99, https://doi.org/10.17804/2410-9908.2018.6.090-099.
[42] E. Pellicer, S. Pané, K.M. Sivaraman, O. Ergeneman, S. Suriñach, M.D. Baró, B.J. Nelson, J. Sort, Effects of the anion in glycine-containing electrolytes on the mechanical properties of electrodeposited Co-Ni films, Mater. Chem. Phys. 130 (2011) 1380–1386, https://doi.org/10.1016/j.matchemphys.2011.09.032.
[43] S. Chikazumi, Physics of Ferromagnetism (2009).
[44] R. Ranchal, S. Fin, D. Bisero, Magnetic microstructures in electrodeposited $Fe_{1-x}Ga_x$ thin films ($15 \leq x \leq 22$ at.%), J. Phys. D: Appl. Phys. 48 (2015) 75001, https://doi.org/10.1088/0022-3727/48/7/075001.
[45] P. Bartolomé, M. Maicas, R. Ranchal, Out of plane component of the magnetization of sputtered $Fe_{72}Ga_{28}$ layers, J. Magn. Magn. Mater. 514 (2020), https://doi.org/10.1016/j.jmmm.2020.167183 167183.
[46] J. Grangle, G.M. Goodman, The magnetization of pure iron and nickel, Proc. Roy. Soc. Lond. A. 321 (1971) 477–491.
[47] V.A. Lukshina, D.A. Shishkin, A.R. Kuznetsov, N.V. Ershov, Y.N. Gornostyrev, Effect of Magnetic Field Annealing on Magnetic Properties of Iron-Gallium Alloys, Phys. Solid State. 62 (2020) 1746–1754, https://doi.org/10.1134/S1063783420100182.
[48] J.M. Borrego, J.S. Blázquez, C.F. Conde, A. Conde, S. Roth, Structural ordering and magnetic properties of arc-melted FeGa alloys, Intermetallics. 15 (2007) 193–200, https://doi.org/10.1016/j.intermet.2006.05.007.
[49] E.E. Moore, P.E.A. Turchi, A. Landa, P. Söderlind, B. Oudot, J.L. Belof, S.A. Stout, A. Perron, Development of a CALPHAD thermodynamic database for Pu-U-Fe-Ga alloys, Appl. Sci. 9 (2019) 5040, https://doi.org/10.3390/app9235040.
[50] F. Zhao, S. Franz, A. Vicenzo, M. Bestetti, F. Venturini, P.L. Cavallotti, Electrodeposition of Fe-Ga thin films from eutectic-based ionic liquid, Electrochim. Acta. 114 (2013) 878–888, https://doi.org/10.1016/j.electacta.2013.07.172.
[51] S.M. Reddy, J.J. Park, S.M. Na, M.M. Maqableh, A.B. Flatau, B.J.H. Stadler, Electrochemical synthesis of magnetostrictive Fe-Ga/Cu multilayered nanowire arrays with tailored magnetic response, Adv. Funct. Mater. 21 (2011) 4677–4683, https://doi.org/10.1002/adfm.201101390.
[52] Q. Xing, Y. Du, R.J. McQueeney, T.A. Lograsso, Structural investigations of Fe-Ga alloys: Phase relations and magnetostrictive behavior, Acta Mater. 56 (2008) 4536–4546, https://doi.org/10.1016/j.actamat.2008.05.011.
[53] I.S. Golovin, V.V. Palacheva, A.K. Mohamed, A.M. Balagurov, Structure and Properties of Fe–Ga Alloys as Promising Materials for Electronics, Phys. Met. Metallogr. 121 (2020) 851–893, https://doi.org/10.1134/S0031918X20090057.
[54] L.R. Nivedita, P. Manivel, R. Pandian, S. Murugesan, N.A. Morley, K. Asokan, R.T. Rajendra Kumar, Enhancement of magnetostrictive properties of Galfenol thin films, J. Magn. Magn. Mater. 451 (2018) 300–304, https://doi.org/10.1016/j.jmmm.2017.11.030.
[55] A. Muñoz-Noval, E. Salas-Colera, R. Ranchal, Local and Medium Range Order Influence on the Magnetic Behavior of Sputtered Ga-Rich FeGa Thin Films, J. Phys. Chem. C. 123 (2019) 13131–13135, https://doi.org/10.1021/acs.jpcc.9b01889.
[56] O. Ikeda, R. Kainuma, I. Ohnuma, K. Fukamichi, K. Ishida, Phase equilibria and stability of ordered b.c.c. phases in the Fe-rich portion of the Fe-Ga system, J. Alloys Compd. 347 (2002) 198–205, https://doi.org/10.1016/S0925-8388(02)00791-0.
[57] A.K. Mohamed, V.V. Palacheva, V.V. Cheverikin, E.N. Zanaeva, W.C. Cheng, V. Kulitckii, S. Divinski, G. Wilde, I.S. Golovin, The Fe–Ga phase diagram: Revisited, J. Alloys Compd. 846 (2020), https://doi.org/10.1016/j.jallcom.2020.156486 156486.
[58] E. Budevski, G. Staikov, W.J. Lorenz, Electrocrystallization Nucleation and growth phenomena, Electrochim. Acta. 45 (2000) 2559–2574, https://doi.org/10.1016/S0013-4686(00)00353-4.
[59] E.P. Georgiou, T. Van der Donck, J.P. Celis, Electrodeposition and structural characteristics of intermetallic nickel-tin based coatings, Trans. Inst. Met. Finish. 95 (2017) 301–307, https://doi.org/10.1080/00202967.2017.1352125.
[60] A. Stephen, F. Rossi, L. Nasi, C. Ferrari, N. Ponpandian, M.V. Ananth, V. Ravichandran, Induced ordering in electrodeposited nanocrystalline Ni-Mn alloys, J. Appl. Phys. 103 (2008) 53511, https://doi.org/10.1063/1.2844211.
[61] S. Ge, Q. Lin, S. Wodarz, M. Kambe, T. Homma, G. Zangari, Electrodeposition of Fe-Ni-Pt alloy films for heat-assisted magnetic recording media: Synthesis, structure and magnetic properties, Electrochim. Acta. 302 (2019) 92–101, https://doi.org/10.1016/j.electacta.2019.01.176.
[62] T. Tsuda, C.L. Hussey, G.R. Stafford, J.E. Bonevich, Electrochemistry of Titanium and the Electrodeposition of Al-Ti Alloys in the Lewis Acidic Aluminum Chloride–1-Ethyl-3-methylimidazolium Chloride Melt, J. Electrochem. Soc. 150 (2003) C234–C243, https://doi.org/10.1149/1.1554915.
[63] F. Meneses, A. Pedernera, C. Blanco, N. Bajales, S.E. Urreta, P.G. Bercoff, L10-FeNi ordered phase in AC electrodeposited iron-nickel biphasic nanowires, J. Alloys Compd. 766 (2018) 373–381, https://doi.org/10.1016/j.jallcom.2018.06.307.
[64] C.-W. Nan, Y. Huang, G.J. Weng, Effect of porosity on the effective magnetostriction of polycrystals, J. Appl. Phys. 88 (2000) 339, https://doi.org/10.1063/1.373664.
[65] C.W. Nan, Physics of inhomogeneous inorganic materials, Prog. Mater. Sci. 37 (1993) 1–116, https://doi.org/10.1016/0079-6425(93)90004-5.
[66] R.F. Pettifer, X-ray Studies of Magnetostriction, in: M.R.J. Gibbs (Ed.), Mod. Trends Magnetostriction Study Appl., Springer Netherlands, Dordrecht, 2001: pp. 249–262. doi:10.1007/978-94-010-0959-1_12.
[67] E. Arakawa, K.I. Maruyama, K. Mori, H. Nishigaitsu, N. Aizawa, Internal magnetostriction observed by X-ray diffraction in iron, IEEE Trans. Magn. 41 (2005) 3718–3720, https://doi.org/10.1109/intmag.2005.1464349.
[68] A. Fujita, K. Fukamichi, K. Koyama, K. Watanabe, X-ray diffraction study in high magnetic fields of magnetovolume effect in itinerant-electron metamagnetic $La(Fe_{0.88}Si_{0.12})_{13}$ compound, J. Appl. Phys. 95 (2004) 6687–6689, https://doi.org/10.1063/1.1667455.
[69] E. Arakawa, K. Mori, H. Nishigaitsu, N. Aizawa, X-ray diffraction technique to observe magnetostriction and magnetization at coextensive volumes of iron, IEEE Trans. Magn. 42 (2006) 81–83, https://doi.org/10.1109/TMAG.2005.859440.
[70] Z. Nie, Z. Wang, Y. Liang, D. Cong, G. Li, C. Zhu, C. Tan, X. Yu, Y. Ren, Y. Wang, Structural investigations of Fe-Ga alloys by high-energy x-ray diffraction, J. Alloys Compd. 763 (2018) 223–227, https://doi.org/10.1016/j.jallcom.2018.05.327.